

Devon: Deformable Volume Network for Learning Optical Flow

Yao Lu*
Data61, ANU

Jack Valmadre
University of Oxford

Heng Wang
Facebook

Juho Kannala
Aalto University

Mehrtash Harandi
Data61, ANU

Philip H. S. Torr
University of Oxford

Abstract

We propose a lightweight neural network model, *Deformable Volume Network (Devon)* for learning optical flow. *Devon* benefits from a multi-stage framework to iteratively refine its prediction. Each stage is by itself a neural network with an identical architecture. The optical flow between two stages is propagated with a newly proposed module, the *deformable cost volume*. The *deformable cost volume* does not distort the original images or their feature maps and therefore avoids the artifacts associated with warping, a common drawback in previous models. *Devon* only has one million parameters. Experiments show that *Devon* achieves comparable results to previous neural network models, despite of its small size.

1. Introduction

Optical flow estimation is the problem of finding pixel motions between two images. It is a classic computer vision problem and has been studied for more than 30 years. Since Horn and Schunck’s variational method [14], a large number of optical flow algorithms [2, 9, 10] has been developed. Nevertheless, the problem of estimating optical flow is not yet solved. One can even claim that we still do not have a practical algorithm which is fast, robust and accurate for real-world images.

Recently, learning optical flow with neural networks has shown great promises [8, 15, 22, 26, 28, 29]. With graphics engines, large scale datasets with synthetic images and ground-truth optical flow are generated [4, 8, 21], which enables end-to-end learning optical flow. We note that while training images are synthetic, neural networks seem to generalize well on real-world images [15]. Compared to classic methods, the neural network approaches have the advantage of offering robust features and fast inference. For example, models in [15] have a running speed from 8-140fps and accuracy competitive with the state-of-the-art methods.

*Corresponding author. Email: yaolubrain@gmail.com

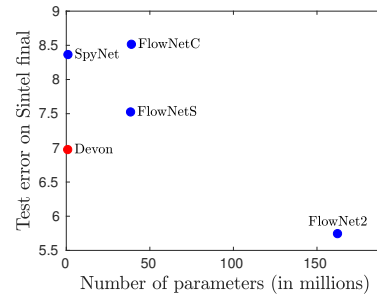


Figure 1. Model size versus test error on the Sintel benchmark.

One of the major difficulties in estimating optical flow is large displacements. Learning optical flow with large displacements cannot be achieved by traditional Convolutional Neural Networks (CNNs). This is due to the fact that CNNs make use of small filters. Obviously, one cannot afford to increase filter sizes naïvely to cover large displacements, as the number of parameters and the computational cost both increase drastically.

To handle large displacements, multi-resolution representations are employed in several neural network models. SpyNet [22] downsamples the original images into multiple scale levels and each level is handled by a CNN. FlowNet [8] and FlowNet2 [15] downsample the feature maps by striding during convolution. As a result, a convolution layer in CNNs that receives lower resolution feature maps has effectively larger receptive size. However, downsampling may lead to loss of valuable information such as small objects and detailed textures. To compensate for such a loss, one needs to increase the number of filters, as suggested in [8, 15, 26]. However, this will inevitably increase the number of parameters. For example, FlowNet2 has over 150 million parameters [15].

Another technique to handle large displacements in neural network models such as [15, 22, 26] is warping, which propagates optical flow between two stages in a model. However, warping often creates distortions and artifacts. This issue will be discussed in details in §2.

In this paper, we introduce Deformable Volume Network (Devon), which avoids the drawbacks of multi-resolution representation and warping. Our main contribution is a newly proposed neural network module, the deformable cost volume, which can propagate optical flow from one stage to another without distorting the original images or their feature maps. We extensively use the idea of dilation in the cost volumes and in convolutions to handle large displacements. As a result, Devon is fully convolutional and does not require the input image to have size a multiple of two. Devon has only one million parameters, which is a significant reduction compared with previous models such as FlowNet, as shown in Figure 1.

2. The Problem of Warping

Warping has been used in variational methods [3, 20] and neural network models [15, 22, 26] for iteratively refining optical flow estimations in a multi-stage framework. The first stage covers large displacements and outputs a rough estimation. Then the second image (or its feature maps) is warped by the roughly estimated optical flow such that pixels of large displacements in the second image are moved closer to their correspondences in the first image. As a result, the next stage, which receives the original first image and the warped second image as inputs, only needs to handle smaller displacements and refines the estimation.

Let $I : \mathbb{R}^2 \rightarrow \mathbb{R}^3$ denote the first image, $J : \mathbb{R}^2 \rightarrow \mathbb{R}^3$ denote the second image and $F : \mathbb{R}^2 \rightarrow \mathbb{R}^2$ denote the optical flow field of the first image. The warped second image is defined as

$$\tilde{J}(\mathbf{p}) = J(\mathbf{p} + F(\mathbf{p})) \quad (1)$$

for image location $\mathbf{p} \in \mathbb{R}^2$ [15].

The warping operation creates a transformed image reasonably well if the new pixel locations $\mathbf{p} + F(\mathbf{p})$ do not occlude or collide with each other. For example, affine transform $F(\mathbf{p}) = \mathbf{A}\mathbf{p} + \mathbf{t}$ where \mathbf{A} and \mathbf{t} are the transformation parameters. However, for real-world images, occlusions are common (e.g. when an object moves and the background is still). If an image is warped with the optical flow which induces occlusions, duplicates will be created.

The effect is demonstrated in Figure 2. The artifacts cannot be cleaned simply by subtracting the first or the second image from the warped image, as shown in Figure 2 (e) and (f).

Intuitively, imagine a pixel which is moved by warping to a new location. If no other pixel are moved to fill in its old location, the pixel will appear twice in the warped image.

Mathematically, consider the following example. Assume the value of $J(\mathbf{p}_1)$ is unique in J , that is, $J(\mathbf{p}) \neq J(\mathbf{p}_1)$ for all $\mathbf{p} \neq \mathbf{p}_1$. Then for an optical flow field in

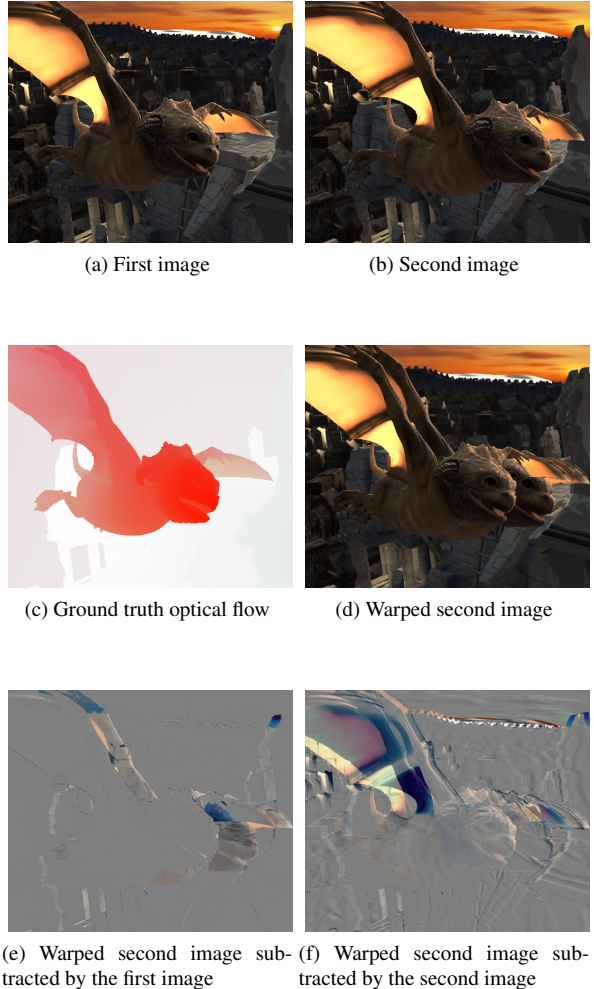


Figure 2. Artifacts of using image warping. From (d), we can see the duplicates of the dragon head and wings. The images and the ground truth optical flow are from the Sintel dataset [4]. Warping is done with function `image.warp()` in the Torch-image toolbox.

which

$$F(\mathbf{p}_1) = 0, \quad F(\mathbf{p}_2) = \mathbf{p}_1 - \mathbf{p}_2, \quad (2)$$

we have

$$\tilde{J}(\mathbf{p}_1) = J(\mathbf{p}_1 + F(\mathbf{p}_1)) \quad (3)$$

$$= J(\mathbf{p}_1 + 0) = J(\mathbf{p}_1), \quad (4)$$

$$\tilde{J}(\mathbf{p}_2) = J(\mathbf{p}_2 + F(\mathbf{p}_2)) \quad (5)$$

$$= J(\mathbf{p}_2 + \mathbf{p}_1 - \mathbf{p}_2) = J(\mathbf{p}_1). \quad (6)$$

Therefore $\tilde{J}(\mathbf{p}_1) = \tilde{J}(\mathbf{p}_2) = J(\mathbf{p}_1)$. Since the value of $J(\mathbf{p}_1)$ is unique in image J but not unique in \tilde{J} , a duplicate is created on the warped second image \tilde{J} .

When the duplicates happen, it makes the optical flow estimation erroneous since artificial candidate correspondences are created. One might argue that neural networks are universal approximators and since they are trained end-to-end with ground-truth optical flow, neural networks can learn the self-corrected correspondences. However, it is not an ideal situation and makes the training more difficult and the neural networks less interpretable.

3. Deformable Cost Volume

Let I denote the first image, J denote the second image and $f_I : \mathbb{R}^2 \rightarrow \mathbb{R}^d$ and $f_J : \mathbb{R}^2 \rightarrow \mathbb{R}^d$ denote their feature maps of dimensionality d , respectively. The standard cost volume is defined as

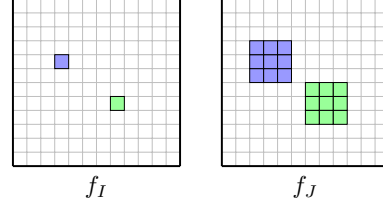
$$C(\mathbf{p}, \mathbf{v}) = \|f_I(\mathbf{p}) - f_J(\mathbf{p} + \mathbf{v})\|, \quad (7)$$

for image location $\mathbf{p} \in \mathbb{R}^2$, neighbor $\mathbf{v} \in [-\frac{k-1}{2}, \frac{k-1}{2}]^2$ of neighborhood size k and a given vector norm $\|\cdot\|$.

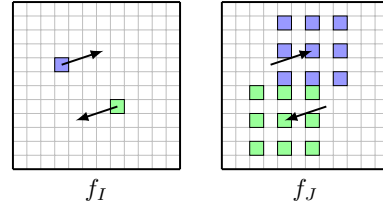
The cost volume gives an explicit representation of displacements. The idea of using cost volume goes back to stereo matching [25]. When using the feature maps learned by neural networks, construction and processing of a fully connected cost volume, in which the neighborhood is large enough to cover the maximum displacement, leads to high performance in stereo matching [35] and optical flow [33]. However, the displacements in stereo matching are one-dimensional while in optical flow they are two-dimensional. For two images (and their feature maps) of resolution $m \times n$, the construction of the cost volume in equation (7) has time and space complexity $O(mndk^2)$. Naïvely increasing neighborhood size k to cover large displacements increases the computation quadratically. As a result, DCFlow requires several seconds to compute optical flow for a pair of images on a GPU and large memory usage [33].

To reduce the computational burden, one can embed the cost volume in a multi-scale representation. In PWC-Net [26], multi-scaled feature maps of two images are created and a cost volume of a small neighborhood is constructed at each scale level. A decoding module at each scale level infers the optical flow from the cost volume representation of displacements and the feature maps of the first image. The optical flow estimated at a coarse level is then upsampled and used to warp the feature maps of the second image at a fine level. As a result, large displacements are estimated at a coarse level and the estimation is propagated to a fine level.

However, as discussed in §2, warping induces artifacts and distortion. To avoid the drawbacks of warping, we propose a new neural network module, the deformable cost volume. The key idea is: instead of deforming images or their feature maps, as done with warping, we deform the cost volume and leave the images and the feature maps unchanged.



(a) Standard cost volume. For each location on the feature maps of the first image, the matching costs of a neighborhood of the same location on the feature maps of the second image are computed.



(b) Deformable cost volume. For each location on the feature maps of the first image, the matching costs of a **dilated** neighborhood of the same location, **offset by a flow vector**, on the feature maps of the second image are computed.

Figure 3. Cost Volumes

The proposed deformable cost volume is defined as

$$C(\mathbf{p}, \mathbf{v}, r, F) = \|f_I(\mathbf{p}) - f_J(\mathbf{p} + r \cdot \mathbf{v} + F(\mathbf{p}))\| \quad (8)$$

where r is the dilation factor and $F(\cdot)$ is an external flow field. The dilation factor r is introduced to enlarge the size of the neighborhood to handle large displacements without increasing computation significantly. This is inspired by the dilated convolution [5, 34] which enlarges its receptive field in a similar way. $F(\cdot)$ can be obtained from the optical flow estimated from a previous stage or an external algorithm. If $F(\mathbf{p}) = 0$ for all \mathbf{p} and $r = 1$, then the deformable cost volume is reduced to the standard cost volume. For non-integer $F(\mathbf{p})$, bilinear interpolation is used. The deformable cost volume is illustrated in Figure 3.

Since the deformable cost volume does not distort f_I or f_J , the artifacts associated with warping will not be created. Optical flow can be inferred from the deformable cost volume solely without resorting to the feature maps of the first image to counter the duplicates.

The deformable cost volume is differentiable with respect to $f_I(\mathbf{p})$ and $f_J(\mathbf{p} + r \cdot \mathbf{v} + F(\mathbf{p}))$ for each image location \mathbf{p} . Due to bilinear interpolation, the deformable cost volume is also differentiable with respect to $F(\mathbf{p})$, using the same technique as in [15, 16]. Therefore, the deformable cost volume can be inserted in a neural network for end-to-end learning optical flow.

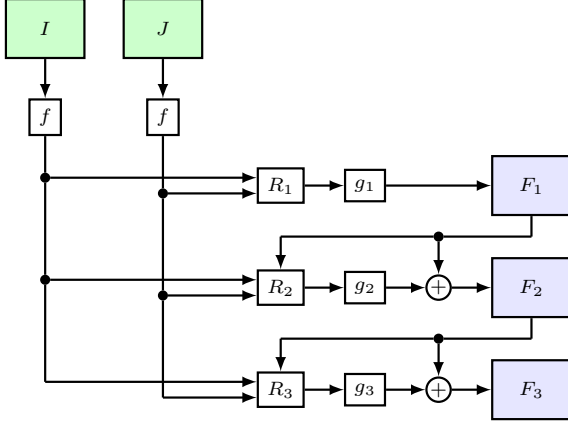


Figure 4. Deformable Volume Network (Devon) with three stages. I denotes the first image, J denotes the second image, f denotes the shared feature extraction module (§4.1), R_t denotes the relation module (§4.2), g_t denotes the decoding module (§4.3) and F_t denotes the estimated optical flow for stage t .

4. Deformable Volume Network

Our proposed model is the deformable volume network (Devon), as illustrated in Figure 4. Devon has multiple stages. Each stage is handled by a neural network with an identical Siamese architecture, which is consisted of a shared feature extraction module, a relation module and a decoding module. The optical flow estimated from a previous stage is propagated to the current one through the deformable cost volume and residual connections. Devon performs iterative refinement such that each stage refines the optical flow estimated by the previous stage.

Compared to previous neural network models [8, 15, 22, 26], Devon has several major differences: (1) All feature maps in Devon have the same resolution. No repeated up/down-sampling is used. This significantly reduces the number of parameters. As mentioned in Section 1, since downsampling with strided convolution reduces resolution, one often has to increase of number of filters so as not to lose information. It also eases the implementation since the input images do not need to have size of a multiple of two. (2) Each stage computes on the undistorted images. No warping is used. (3) The decoding module only receives inputs from the relation module. Therefore, neural networks infer the optical flow solely from the relations between two images, rather than memorize the optical flow pattern of a single image as a short-cut. The short-cut issue has appeared when applying neural networks to learn monocular stereo [30]. On the contrary, in FlowNetC and PWC-Net the decoding module also receives inputs from their feature extraction module of the first image. (4) All stages share the feature extraction module. This reduces the number of parameters and computation time further.

We describe the details of each module structure below. All convolution layers are fully convolutional, that is, having stride 1 and zero-padding $\frac{k-1}{2}$ where k is the filter size. Besides, all convolution layers, except the last one in the feature extraction module and the last one in the decoding module, are followed by a leaky ReLU function [12] with leakiness 0.1.

4.1. Feature Extraction Module

We use a very simple feature extraction module, a three-layer fully convolutional network, as shown in Figure 5. This module is similar to the feature extraction module in DCFlow [33].

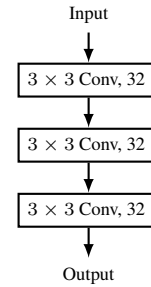


Figure 5. Feature extraction module f . For Conv layer, the number of filter is specified on the right.

4.2. Relation Module

In the relation module, to handle multi-scale motion, we concatenate the outputs of three deformable cost volumes, which have different neighborhood size k or dilation factor r . When the module does not receive an optical flow as one of the inputs, it is set to receive a zero-valued optical flow field.

Next, for each location in the concatenated feature maps, a normalization method is applied across the channels. We choose softmax function, which encourages the channel with the minimum cost to pop-up. The comparison of different normalization methods is in §6.4.2; The whole module structure is illustrated in Figure 6.

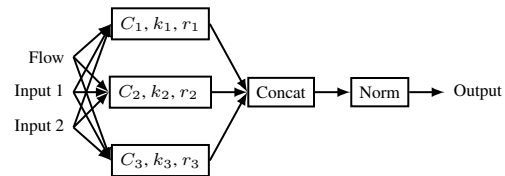


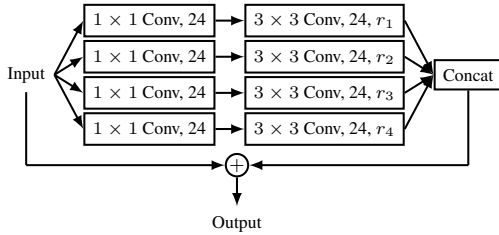
Figure 6. Relation module R . C_1 , C_2 and C_3 denote the deformable cost volumes. k_1 , k_2 and k_3 denote the neighborhood sizes. r_1 , r_2 and r_3 denote the dilation factors. Concat denotes concatenation. Norm denotes normalization.

We use hyper-parameters $(k_1, k_2, k_3) = (5, 5, 7)$ and $(r_1, r_2, r_3) = (1, 3, 9)$. Such combination enables dense correspondences nearby an image location and sparse correspondences faraway. This is consistent to the fact that small displacements are more frequent in natural videos [24] and resembles the structure of retina.

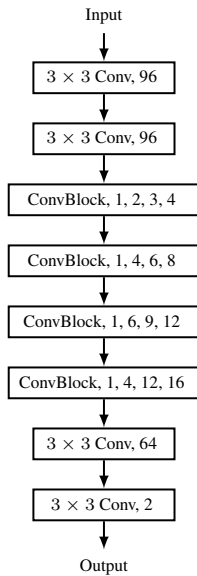
The output of this module has size $(k_1^2 + k_2^2 + k_3^2) \times m \times n$, where m is height and n is the width of the feature maps.

4.3. Decoding Module

In the decoding module, we use a fully convolutional network with residual connections [13] and dilated convolution [5, 34]. We use dilated convolution with dilation factors from 2 to 16 to enlarge the receptive fields. The convolution block as in Figure 7 (a) allows multi-scale processing, which has been shown effective in semantic segmentation [6]. The 1×1 convolutions [18] are used in here for efficient computation, as in [27]. The residual connection facilitates training, as demonstrated in [13, 27]. The whole module structure is illustrated in Figure 7 (b).



(a) ConvBlock. r_1, r_2, r_3, r_4 are dilation factors.



(b) Module Structure. For ConvBlock layer, the dilation factors are specified on the right.

Figure 7. Decoding module g

5. Training

We train Devon end-to-end with the following loss function

$$L = \sum_t \gamma_t |F_{GT} - F_t|_1 \quad (9)$$

where F_{GT} denotes the ground-truth optical flow and F_t denotes the estimated optical flow at stage t . For Devon with three stages, we choose $\gamma_1 = 0.2, \gamma_2 = 0.3$ and $\gamma_3 = 0.5$. We use l_1 loss instead of l_2 loss for more robustness. All pixel values of the images are multiplied by $2/255$ and subtracted by 1 to have range $[-1, 1]$. Empirically, such normalization is found to accelerate the training.

For optimization algorithm, we use Adam [17] with $\beta_1 = 0.9, \beta_2 = 0.999$ and $\epsilon = 10^{-8}$. However, instead of using a carefully tuned learning rate schedule as in [15, 26], we use a very simple schedule: starting from learning rate $\alpha = 10^{-3}$, multiply by 0.8 for every 20000 mini-batch updates of size 9. We use the weight initialization method in [12]. All biases are initialized to be zero.

Instead of using the intensive data augmentation as in [8], we use a simple data augmentation which is consisted of random cropping, horizontal flipping, vertical flipping and color channel random shuffling.

6. Experiments

We evaluate Devon on three benchmarks: FlyingChairs [8], Sintel [4] and KITTI [11], as in [8, 22, 15, 26]. We compare Devon with the previous neural network models: FlowNetS [8], FlowNetC [8], FlowNet2 [15], SpyNet [22] and PWC-Net [26]. We use Devon with three stages. All stages have the identical architecture and hyper-parameters, as described in §4. We use l_1 norm for the deformable cost volumes.

6.1. FlyingChairs

We train Devon on the FlyingChairs training set, following the procedure in §5, and evaluate it on the FlyingChairs validation set. The train/valid split is followed from [8]. All images are $4 \times$ downsampled. For training, the ground-truth optical flow are also $4 \times$ downsampled. In evaluation, the computed optical flows are $4 \times$ upsampled. This reduces the computation time by a large amount without losing accuracy significantly. In data augmentation during training, we use random cropping with size 112×80 . The results are listed in Table 3. As FlowNet2 has many variants, the result for FlowNet2 is the lowest average end-point error found in the original paper [15]. For qualitative assessment, we visualize results in Figure 8. The image were selected from the FlyingChairs validation set. No fine-tuning was applied to any model. From the results, we can see Devon outperforms FlowNetS, FlowNetC, SpyNet and PWC-Net.

6.2. Sintel

For the evaluation on Sintel, we train Devon on the training set of FlyingChairs [8], FlyingThings3D [21] and ChairsSDHom [15], as in [15]. However, instead of using a carefully designed dataset schedule (FlyingChairs \rightarrow FlyingThings3D \rightarrow ChairsSDHom) as in [15], we simply train Devon on the three datasets simultaneously, following the procedure in §5, with a mini-batch of size 9, which contains 3 samples from each dataset. For fine-tuning on the Sintel training set (mixture of clean and final), we use learning rate 10^{-5} without learning rate decay, mini-batch size 4 and random cropping of size 192×96 . All images and the ground-truth optical flow are $4\times$ downsampled. In evaluation, the computed optical flows are $4\times$ upsampled. The results are listed in Table 3 and visualized in Figure 9. From the results, we can see Devon outperforms FlowNetS, FlowNetC and SpyNet.

6.3. KITTI

As images in KITTI are much wider in size (e.g. 1024×375), we resize the images and the ground-truth optical flow to have size 207×125 . In evaluation, the computed optical flows are upsampled to the size of the original images. We evaluate Devon trained on FlyingChairs, FlyingThings3D and ChairsSDHom and then fine-tuned on the KITTI training set. For fine-tuning on the KITTI training set (mixture of 2012 and 2015), we use learning rate 10^{-5} without learning rate decay, mini-batch size 2 and random cropping of size 196×112 . Since the images in KITTI 2012 are gray-scaled, we extend them to be RGB images by duplicating the gray values in each RGB channel. The results are listed in Table 3 and visualized in Figure 10. Again, from the results, we can see Devon outperforms FlowNetS, FlowNetC and SpyNet.

6.4. Analysis

6.4.1 Model Size and Runtime

We compare the size and runtime of different neural network models. The timing was recorded on a NVIDIA Pascal TitanX for processing a pair of images of size 1024×448 . FlowNetS, FlowNetC and PWC-Net downsample the feature maps with strided convolution, compute the $4\times$ downsampled optical flow and upsample it. However, Devon is fully convolutional and does not perform downsampling inside the network. Therefore, we $4\times$ downsample the images and $4\times$ upsample the computed optical flow, as in the evaluations on FlyingChairs and Sintel. The results are listed in Table 1. Except for Devon and SpyNet, the number are taken from [26], in which the timing was also recorded on the same GPU.

Method	#parameters (M)	Runtime (ms)
FlowNetS	38.67	11.40
FlowNetC	39.17	21.69
FlowNet2	162.49	84.80
PWC-Net	8.75	28.56
SpyNet	1.20	98.99
Devon	1.05	47.09

Table 1. Model size and runtime

6.4.2 Normalization

The normalization in the relation module (described in §2) is vital to performance. Empirically, we found the spatial softmax gives the most accurate results. The results of using different normalization methods under the same model for training and evaluating on FlyingChairs are listed in Table 2.

Method	None	l_2	Softmax	Softmin
AEE	2.68	2.73	3.14	2.01

Table 2. Average end-point error on FlyingChairs validation set.

7. Discussions

As optical flow is a dense prediction problem, we draw inspirations from the semantic segmentation literature [5, 6, 34]. Due to the aperture problem and textureless regions, motion cannot be inferred locally. Therefore, more global context (or large receptive fields) is required for accurate estimation. The use of dilation in deformable cost volume and the decoding module increase the size of receptive field without increasing the number of parameters.

The deformation in deformable cost volume is different from the one in deformable convolutional networks [7]. In deformable cost volume, the cost volume is offset by an external optical flow and dilation. There is no learnable parameter. While in deformable convolutional networks, the deformation is element-wise and the offset parameters are learned during training.

Applying softmax normalization on hidden unit outputs is found advantageous in modeling general image relations [19].

In this paper, we proposed a new neural network model, Deformable Volume Network (Devon) for learning optical flow. Devon is based on the newly proposed neural network module, the deformable cost volume, which explicitly represents displacements and propagates optical flow between previous estimation without the artifacts associated with warping. Experiments demonstrate the effectiveness of Devon in estimating optical flow with large displacements.

	FlyingChairs	Sintel clean		Sintel final		KITTI 2012		KITTI 2015		
	Valid AEE	Train AEE	Test AEE	Train AEE	Test AEE	Train AEE	Test AEE	Train AEE	Train F1-all	Test F1-all
DeepFlow [31]	-	2.66	5.38	3.57	7.21	4.48	5.8	10.63	26.52%	29.18%
EpicFlow [23]	-	2.27	4.12	3.56	6.29	3.09	3.8	9.27	27.18%	27.10%
MRFlow [32]	-	1.83	2.53	3.59	5.38	-	-	-	14.09%	12.19%
FlowFields [1]	-	1.86	3.75	3.06	5.81	3.33	3.5	8.33	24.43%	-
DCFlow [33]	-	-	3.54	-	5.12	-	-	-	15.09%	14.83%
FlowNetS	2.56	4.35	-	5.46	-	8.26	-	-	-	-
FlowNetS (ft)	-	(3.66)	6.96	(4.44)	7.52	-	-	-	-	-
FlowNetC	2.22	3.52	-	5.00	-	9.35	-	-	-	-
FlowNetC (ft)	-	(3.50)	6.85	(3.89)	8.51	-	-	-	-	-
FlowNet2	1.78	2.02	3.96	3.14	6.02	4.09	-	10.06	30.37%	-
FlowNet2 (ft)	-	(1.45)	4.16	(2.01)	5.74	(1.28)	1.8	(2.30)	(8.61%)	10.41%
PWC-Net	2.06	2.59	-	3.98	-	3.98	-	9.76	33.04%	-
PWC-Net (ft)	-	(1.80)	4.34	(2.39)	5.63	(1.83)	2.1	(2.41)	(11.51%)	11.50%
SpyNet	2.63	4.12	6.69	5.57	8.43	9.12	-	-	-	-
SpyNet (ft)	-	(3.17)	6.64	(4.32)	8.36	(4.13)	4.7	-	-	-
Devon	2.01	2.82	-	4.51	-	4.48	-	10.74	34.30%	-
Devon (ft)	-	(1.97)	4.81	(2.67)	6.97	(1.58)	2.7	(2.93)	(15.88%)	22.15%

Table 3. Results. (ft) denotes the fine-tuning. AEE denotes Average Endpoint Error. F1-all denotes the ratio of pixels where flow estimate is incorrect by both ≥ 3 pixels and $\geq 5\%$.

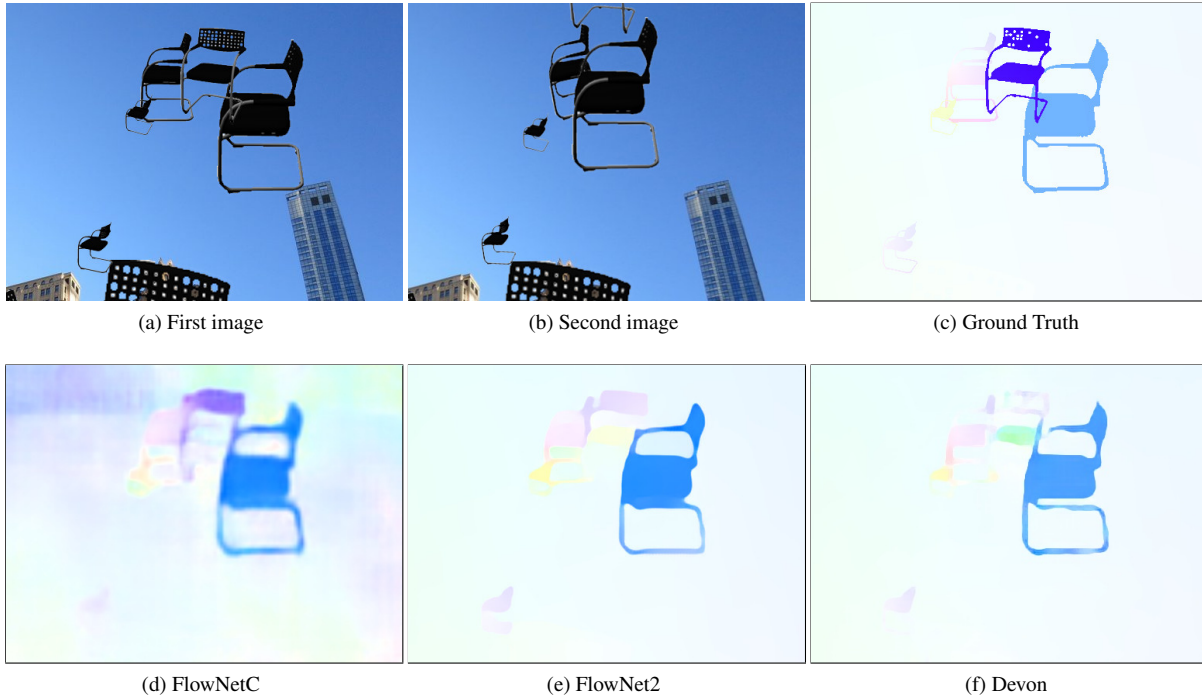


Figure 8. FlyingChairs. Images are selected from the validation set. No fine-tuning was applied.

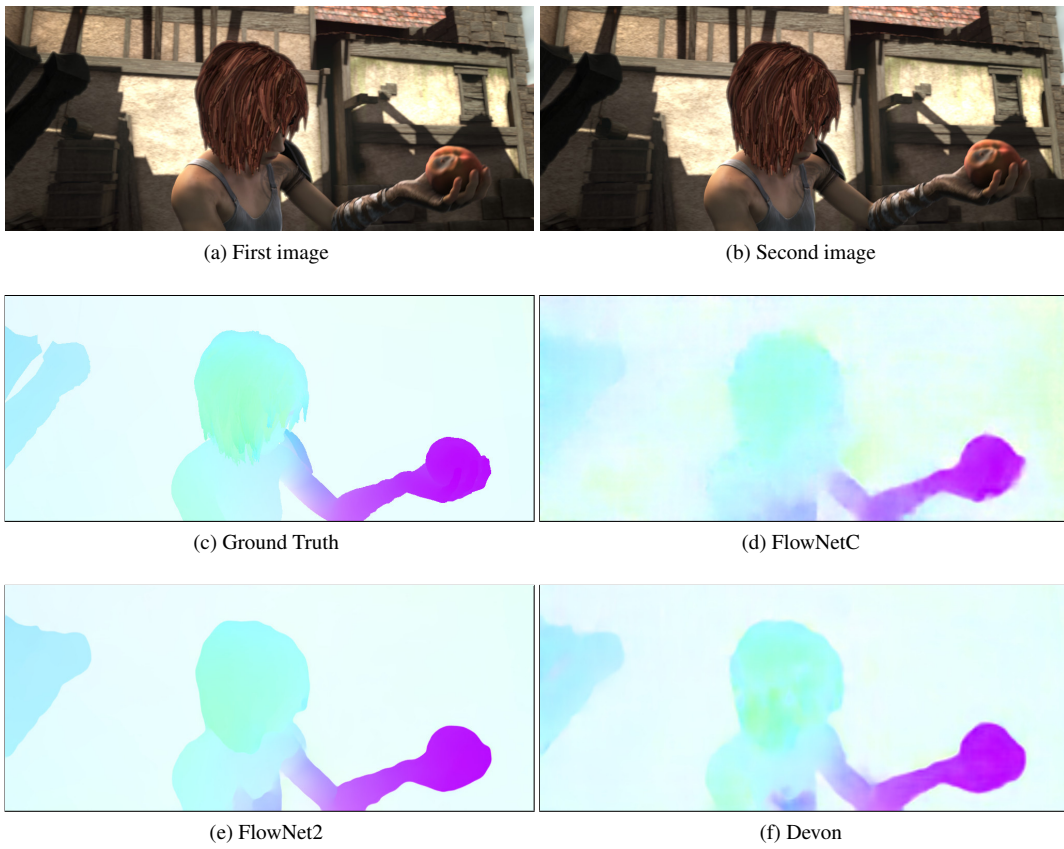


Figure 9. Sintel. Models were trained on FlyingChairs, FlyingThings3D and ChairsSDHom. No fine-tuning was applied.

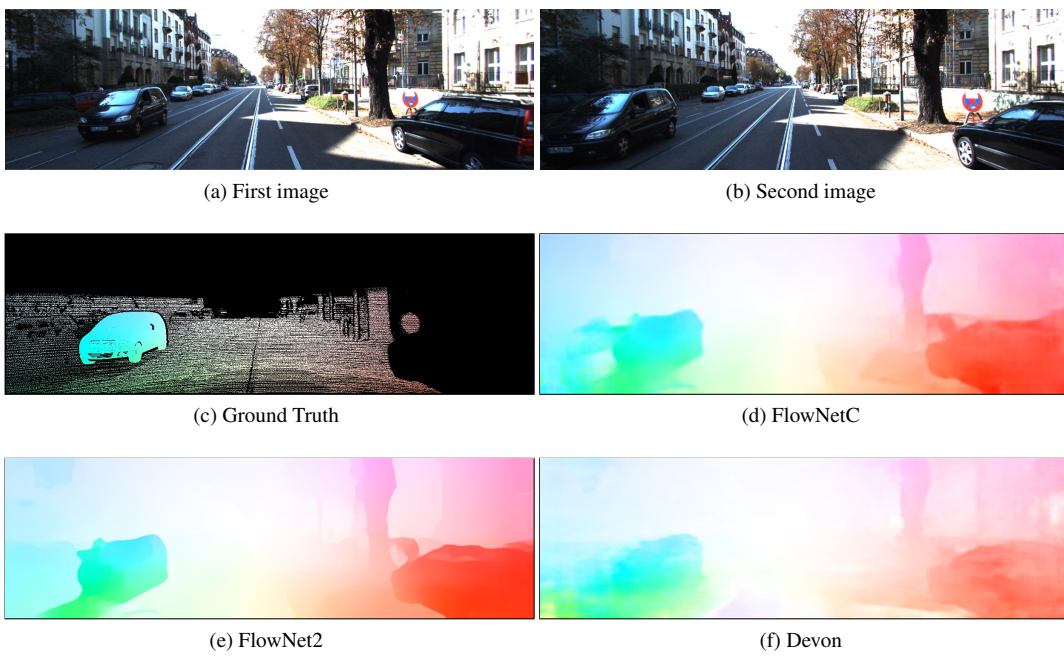


Figure 10. KITTI 2015. Models were trained on FlyingChairs, FlyingThings3D and ChairsSDHom. No fine-tuning was applied.

References

- [1] C. Bailer, B. Taetz, and D. Stricker. Flow fields: Dense correspondence fields for highly accurate large displacement optical flow estimation. *ICCV*, 2015.
- [2] S. S. Beauchemin and J. L. Barron. The computation of optical flow. *ACM computing surveys*, 1995.
- [3] T. Brox, A. Bruhn, N. Papenberg, and J. Weickert. High accuracy optical flow estimation based on a theory for warping. *ECCV*, 2004.
- [4] D. J. Butler, J. Wulff, G. B. Stanley, and M. J. Black. A naturalistic open source movie for optical flow evaluation. *ECCV*, 2012.
- [5] L.-C. Chen, G. Papandreou, I. Kokkinos, K. Murphy, and A. L. Yuille. Deeplab: Semantic image segmentation with deep convolutional nets, atrous convolution, and fully connected crfs. *arXiv*, 2016.
- [6] L.-C. Chen, G. Papandreou, F. Schroff, and H. Adam. Rethinking atrous convolution for semantic image segmentation. *arXiv*, 2017.
- [7] J. Dai, H. Qi, Y. Xiong, Y. Li, G. Zhang, H. Hu, and Y. Wei. Deformable convolutional networks. *ICCV*, 2017.
- [8] A. Dosovitskiy, P. Fischer, E. Ilg, P. Häusser, C. Hazırbaş, V. Golkov, P. van der Smagt, D. Cremers, and T. Brox. FlowNet: Learning optical flow with convolutional networks. *ICCV*, 2015.
- [9] D. Fleet and Y. Weiss. Optical flow estimation. In *Handbook of mathematical models in computer vision*. 2006.
- [10] D. Fortun, P. Bouthemy, and C. Kervrann. Optical flow modeling and computation: a survey. *CVIU*, 2015.
- [11] A. Geiger, P. Lenz, and R. Urtasun. Are we ready for autonomous driving? the kitti vision benchmark suite. *CVPR*, 2012.
- [12] K. He, X. Zhang, S. Ren, and J. Sun. Delving deep into rectifiers: Surpassing human-level performance on imagenet classification. *CVPR*, 2015.
- [13] K. He, X. Zhang, S. Ren, and J. Sun. Deep residual learning for image recognition. *CVPR*, 2016.
- [14] B. K. Horn and B. G. Schunck. Determining optical flow. *Artificial Intelligence*, 1981.
- [15] E. Ilg, N. Mayer, T. Saikia, M. Keuper, A. Dosovitskiy, and T. Brox. FlowNet 2.0: Evolution of optical flow estimation with deep networks. *CVPR*, 2017.
- [16] M. Jaderberg, K. Simonyan, A. Zisserman, et al. Spatial transformer networks. *NIPS*, 2015.
- [17] D. Kingma and J. Ba. Adam: A method for stochastic optimization. *ICLR*, 2014.
- [18] M. Lin, Q. Chen, and S. Yan. Network in network. *arXiv*, 2013.
- [19] Y. Lu, Z. Yang, J. Kannala, and S. Kaski. Learning image relations with contrast association networks. *arXiv*, 2017.
- [20] B. D. Lucas and T. Kanade. An iterative image registration technique with an application to stereo vision. *IJCAI*, 1981.
- [21] N. Mayer, E. Ilg, P. Häusser, P. Fischer, D. Cremers, A. Dosovitskiy, and T. Brox. A large dataset to train convolutional networks for disparity, optical flow, and scene flow estimation. *CVPR*, 2016.
- [22] A. Ranjan and M. J. Black. Optical flow estimation using a spatial pyramid network. *CVPR*, 2017.
- [23] J. Revaud, P. Weinzaepfel, Z. Harchaoui, and C. Schmid. EpicFlow: Edge-Preserving Interpolation of Correspondences for Optical Flow. *CVPR*, 2015.
- [24] S. Roth and M. J. Black. On the spatial statistics of optical flow. *IJCV*, 2007.
- [25] D. Scharstein and R. Szeliski. A taxonomy and evaluation of dense two-frame stereo correspondence algorithms. *IJCV*, 2002.
- [26] D. Sun, X. Yang, M.-Y. Liu, and J. Kautz. Pwc-net: Cnns for optical flow using pyramid, warping, and cost volume. *arXiv*, 2017.
- [27] C. Szegedy, S. Ioffe, V. Vanhoucke, and A. A. Alemi. Inception-v4, inception-resnet and the impact of residual connections on learning. *AAAI*, 2017.
- [28] D. Teney and M. Hebert. Learning to extract motion from videos in convolutional neural networks. *arXiv*, 2016.
- [29] J. Thewlis, S. Zheng, P. H. Torr, and A. Vedaldi. Fully-trainable deep matching. *BMVC*, 2016.
- [30] B. Ummenhofer, H. Zhou, J. Uhrig, N. Mayer, E. Ilg, A. Dosovitskiy, and T. Brox. Demon: Depth and motion network for learning monocular stereo. *arXiv*, 2016.
- [31] P. Weinzaepfel, J. Revaud, Z. Harchaoui, and C. Schmid. Deepflow: Large displacement optical flow with deep matching. *ICCV*, 2013.
- [32] J. Wulff, L. Sevilla-Lara, and M. J. Black. Optical flow in mostly rigid scenes. *CVPR*, 2017.
- [33] J. Xu, R. Ranftl, and V. Koltun. Accurate Optical Flow via Direct Cost Volume Processing. *CVPR*, 2017.
- [34] F. Yu and V. Koltun. Multi-scale context aggregation by dilated convolutions. *ICLR*, 2015.
- [35] J. Zbontar and Y. LeCun. Stereo matching by training a convolutional neural network to compare image patches. *JMLR*, 2016.